# 4 CONSTRAINING DATA

## 4.1 Introduction

Forward density modelling is a very useful tool for testing geological models that represent the Earths interior (e.g. crustal/mantle) structure. It allows the predicted gravity signal from geological bodies with defined features (geometry and density) to be compared with the measured gravity; therefore showing if a geological hypothesis can be accepted. As an interpretation method, due to the ambiguity of solutions of Laplace and Poisson equations, the forward density modelling is not an independent method all by itself. It needs to be constrained by independent geophysical, geological, petrological and geochemical data. The results from other geophysical methods, such as reflection and refraction seismics, seismology, magnetotellurics and receiver function methods produce models that show structures of the Earths interior and their physical parameters (velocities, susceptibilities, depths of boundaries of studied structures, seismicity etc.). From geology, information about structures, tectonic setting, deformation processes taking place in a study area and their morphological expression are derived. From the composition of surface lavas, indications of the composition of subsurface structures can be obtained from petrology and geochemistry. All of this information provides constraints necessary for density modelling.

The additional information used for this model comes from two seismic experiments, the ISSA 2000 and SPOC projects, receiver function studies, magnetotelluric studies (Figure 4.1), velocity–density conversion, density measurements and geological mapping.

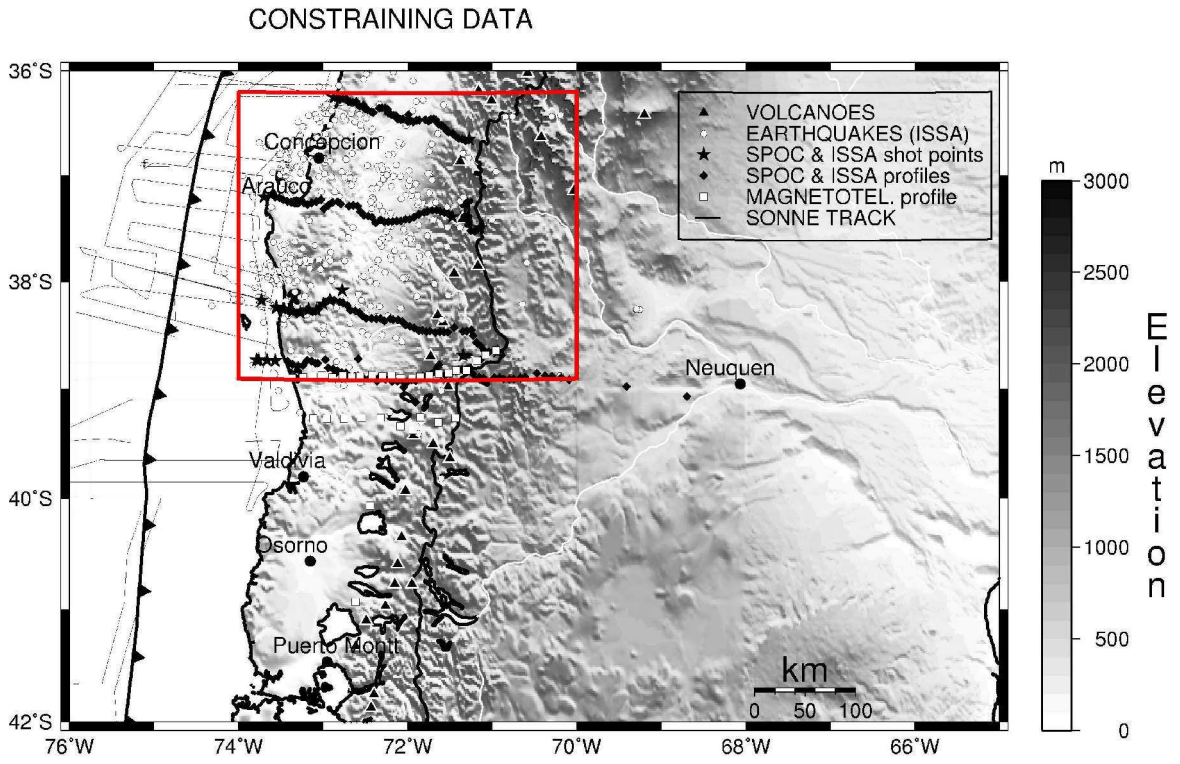


**Figure 4.1**
The constraining data used as additional information for the density model. The SPOC wide angle refraction, near vertical reflection and the ISSA refraction profiles are marked by black diamonds (shot points by black stars). The seismicity based on the ISSA catalogue is denoted by white circles. The area of the local earthquake tomography model is marked by a box.

## *4.2 Geophysical constraints*

### 4.2.1 Data from the ISSA experiment

The Integrated Seismological experiment in the Southern Andes, ISSA 2000, project took place between January and April 2000 between 36°S and 40°S and covered an area of 400 km x 550 km from the Chilean Pacific coast almost to the Argentinean Neuquén Basin (Bohm et al., 2002; Lüth et al., 2003). During these three months, 333 local earthquakes were recorded by a network of 62 onshore seismological stations, together with 15 ocean-bottom hydrophones (OBH) and one ocean bottom seismograph (OBS). The average spacing of the stations was about 50 km. For the simultaneous inversion to produce a 1-D velocity model, the best 120 local events with 1945 P-wave and 1119 S-wave readings were selected (Figure 4.2).

*Seismicity*

The following summary is based on Bohm et al. (2002), unless otherwise stated.

The results of the seismological investigations of the ISSA 2000 project provide the first accurate image of the Benioff zone in the Southern Andes. This zone has a dip of 10°E at longitudes between 73°W and 74°W, and 30° ± 1°E further toward the east. The Benioff zone defines an east-dipping plane with continuous seismicity until 120 km depth (Figure 4.2). In addition, the pattern of seismicity gives an indication of the tectonic activity within the continental plate. The crustal seismicity, with events shallower than 40 km (white circles, Figure 4.2), are concentrated in the forearc region, whereas below the Longitudinal Valley and the Main Cordillera there were less earthquakes recorded during the ISSA measuring period. The earthquakes of the forearc are grouped into two major clusters north and south of the Arauco peninsula along the two major fault zones (Bio-Bio (BB) and south of it the Lahnaluhe (Gastre) Fault Zones (LFZ), Figure 4.2.) The area between them, belonging to the Arauco peninsula and the Nahuelbuta Mountains, is apparently a zone with less crustal seismicity. The depth-frequency distribution obtained by the ISSA network shows two maxima. One is at 20 km depth, reflecting the seismic coupling zone. The second is at 60 km depth and may be associated with the dehydration processes of the subducting Nazca plate (intermediate crustal seismicity in general is associated with metamorphic processes in the crust and upper mantle of the subducting oceanic plate). South of 39°S, the Nazca plate is relatively younger and almost no earthquakes occurred within the slab. This north-to-south decrease in seismicity might be caused by a change in the thermal structure associated with the younging slab.

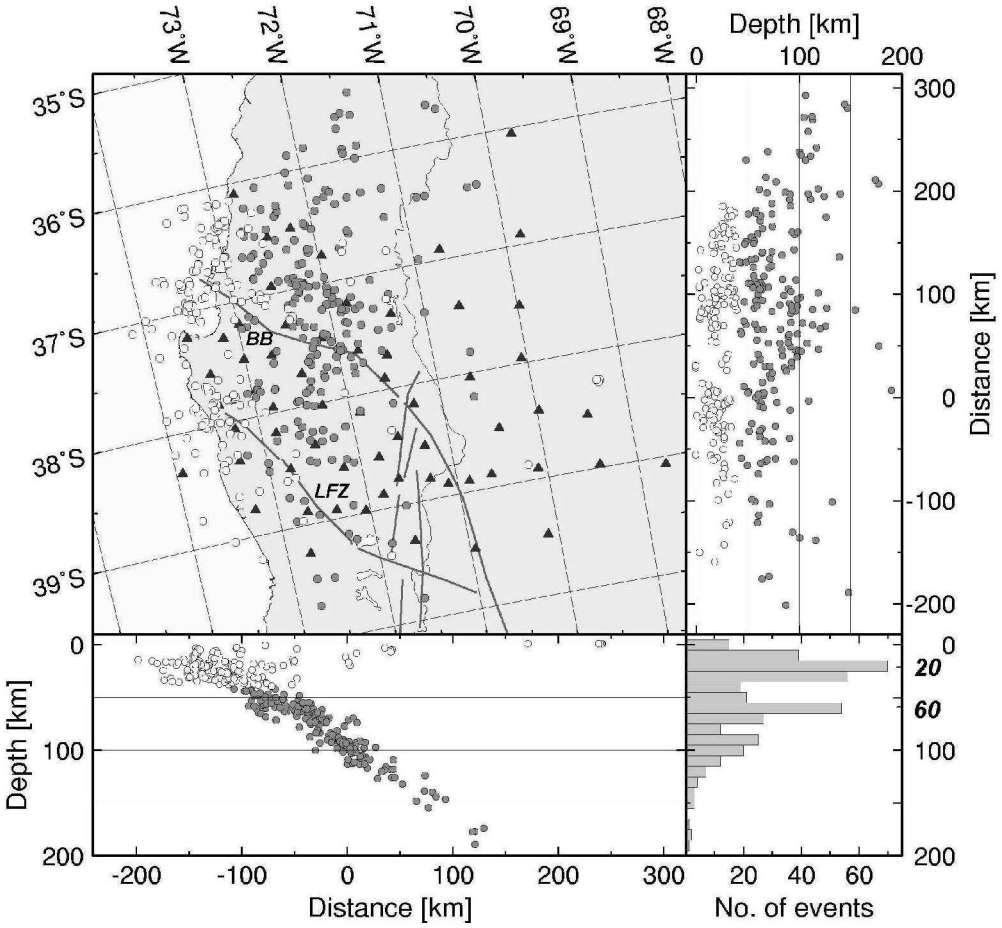


**Figure 4.2**
The distribution of the 333 earthquakes located during the ISSA 2000 experiment (Bohm et al., 2002; Bohm, 2004). The upper-left part of the figure showing earthquake epicentres (crustal seismicity, white circles, and intermediate, below 40 km depth, gray circles) and the stations of the seismic network (black triangles). In the upper-right part are the hypocentres, projected onto a N-S cross-section. The lower-left part shows the hypocentres projected onto an E-W vertical cross-section that define the Benioff zone. To its right is the depth distribution of the earthquakes showing the two maxima at 20 km and 60 km depth.

*1-D velocity model*

In the 1-D velocity model developed from the ISSA project, average P-wave velocities ($v_P$) are 6.3 km/s for the upper crust and 6.9 – 7.4 km/s for the lower crust, indicating felsic to mafic composition. Mantle velocities of 8.0 km/s and 8.34 km/s are observed below 55 km depth and 90 km depth respectively. The $v_P/v_S$ ratio has an average value of 1.75 for both the crust and the mantle. It varies only at the crust/mantle boundary and in the upper 5 km of the crust. A well-pronounced velocity jump of S-wave velocities ($v_S$) at the crust/mantle boundary is observed at the depth of 45 km (Bohm et al., 2002).

*local earthquake tomography model*

The following summary is based on Bohm 2004, unless otherwise stated.

After the 1-D velocity model was developed as the starting and reference model, the 2-D and, subsequently 3-D, velocity models were derived based on travel-time inversion. The 3-D local earthquake tomography model is a regional model reflecting the structures of the study area. Structures identified in the 3-D velocity model are the oceanic crust and mantle and the continental crust below the forearc and the main arc.

Oceanic crust and the mantle region whose geometry is constrained by the Benioff zone seismicity show higher P-wave velocities. At depth of 30-40 km velocities reach values of 7.5 km/s to 7.8 km/s and at greater depths, for instance 110 km, velocities increase to approximately 8.3 km/s.

The 3-D local earthquake tomography model onshore extends until the main volcanic arc (Main Cordillera) and also shows properties of the forearc region – the Coastal Cordillera and the Longitudinal Valley. Velocities of the region underneath the Coastal Cordillera are partly dominated by the high velocities of the oceanic plate, but further east slower values of 6.8 km/s to 7.5 km/s are found at depths of 30-50 km. The area of these slow velocities is especially pronounced in the northern and central parts of the area of interest and is interpreted to be serpentinized uppermost mantle (Figure 4.3). The area beneath the Longitudinal Valley is characterized by high velocities of 7.3 km/s at 30 km depth increasing to 8.1 km/s at a depth of 50 km. Higher velocities below this region are observed along almost entire 300 km north-south length of the study area. Under the magmatic arc, mantle velocities are first observed at depths of 50–55 km.

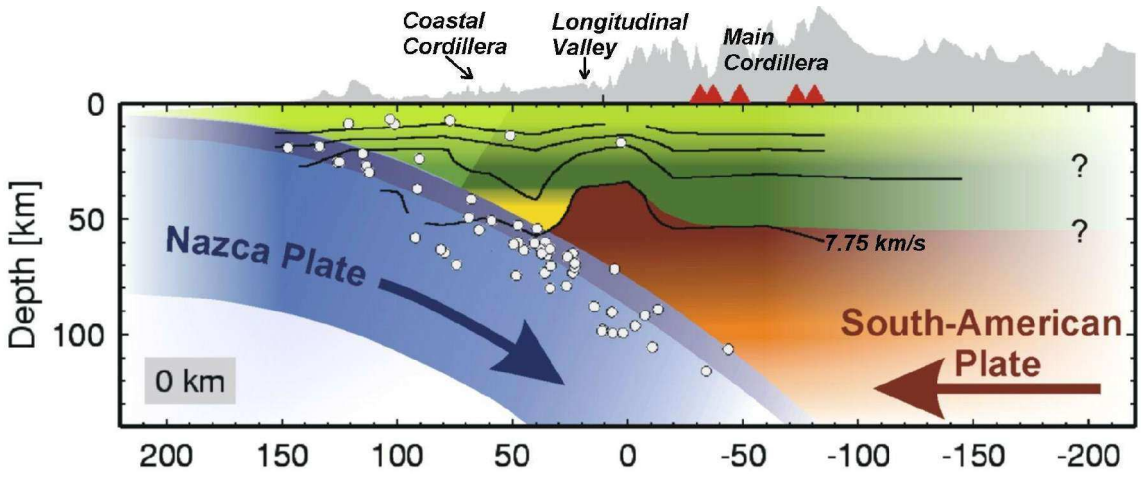


**Figure 4.3**
The final interpretation of the tomography model (Bohm et al., 2003; Bohm, 2004). The crust/mantle boundary is defined by the isoline with a velocity value of 7.75 km/s. The mantle upwelling (brown) below the Longitudinal Valley reaches ~40 km depth; the yellow coloured triangular body is interpreted to represent the serpentinized mantle (low velocity zone) below the forearc Coastal Cordillera. The Moho below the main arc is at ~50-55 km depth.

*2-D velocity model from the seismic refraction profile*

The following summary is based on Lüth et al. 2003, unless otherwise stated.

All of the land stations of the survey were deployed along a profile at 38.8°S. The 2-D crustal velocity model was derived from travel-time forward modelling of the correlated phases on shot sections from 5 shot-points. Four of these shot points were in the Pacific Ocean, and one at a point in the lake in the Chilean Main Cordillera. The 320 km long refraction profile consisted of 62 stations with an average spacing of 4-5 km.

The velocity model is subdivided into the following layers (Figure 4.4). The upper crust shows a layer of unconsolidated sediments of the offshore Valdivia basin (blue colour below the shot points Fig. 4.3), and Neuquén basin onshore in the eastern part of the model. The P-wave velocities here have values of 2.0-5.8 km/s. The upper crust in general is characterized by P-wave velocities of 5.9-6.4 km/s and has a varying thickness along the profile. Below the forearc, it is about 15 km thick, whereas under the magmatic arc, where high velocities are reached at shallow depths, its thickness is only 10 km. The average velocities indicate felsic to intermediate composition of the upper crust. The lower crust thickens from 10 km to

20 km between the forearc and the main arc and has average velocities of 6.6-6.9 km/s. The crust/mantle boundary beneath the volcanic arc is not seen in the refraction profile. However, it was resolved by receiver function studies at a depth of around 40 km (Yuan et al., 2004, submitted). A wedge-shaped structure with P-wave velocity of 7.2 to 7.3 km/s is present underneath the forearc between the lower crust and the oceanic crust. The upper eastern part of this layer shows velocities higher than those beneath the forearc and can be attributed to the continental mantle. The relatively low velocities of the same layer in its western part could be associated with the serpentinization of the continental mantle or the presence of the sediments being subducted from the trench. The oceanic crust under the Coastal Cordillera observed by the refraction seismic profile is resolved until a the depth of 45 km. This layer is 7 km thick, with P-wave velocity changing from 6.9 km/s to 7.2 km/s and showing an eastward dip of around 15°.

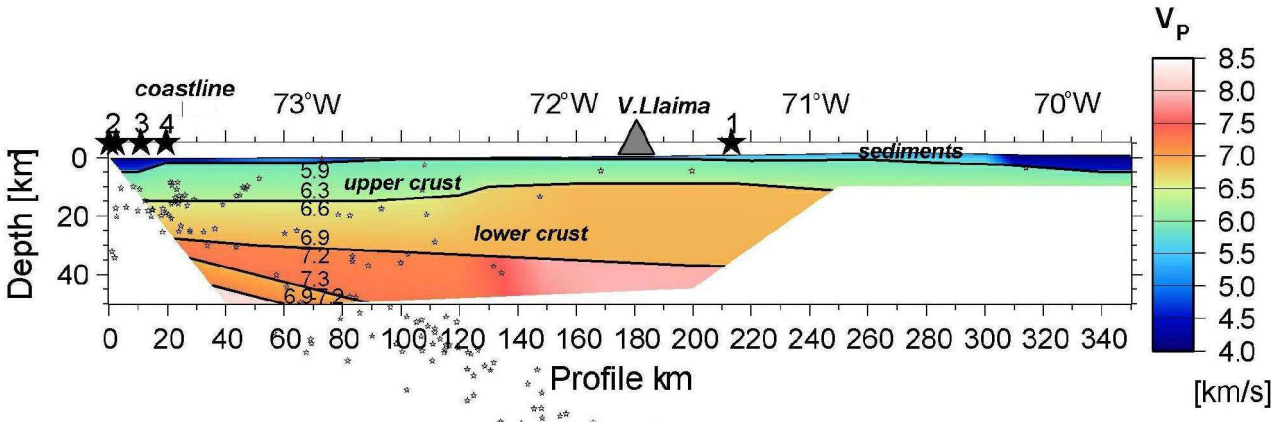


**Figure 4.4**
The 2D refraction velocity model along a profile at 38.8°S, showing a two-layer crust. The low-velocity zones (blue) are observed in the offshore forearc and in the upper crust of the Neuquén basin, associated with sediments (Lüth et al., 2003).

*Receiver function study*

The following summary is based on Yuan et al. 2004 (submitted), unless otherwise stated.

The teleseismic earthquakes recorded during the course of the ISSA experiment were used for a receiver function study. The 13 broadband seismic stations along the 450 km long E-W profile at a latitude of ~39°S were deployed between April 1999 and November 2001. This profile (Figure 4.5) runs from the

Pacific Ocean to the Neuquén basin, cutting across the main three morphotectonic units of the study area (the forearc, the arc and the backarc). The slab is traced till 100 km depth, but it is not visible below the volcanic arc. The continental Moho is imaged at 40 km depth below the main cordillera. Its depth decreases both to the east and west. To the west it shallows to ~25 km depth below the Longitudinal Valley (below the station AS05, Figure 4.5). To the east it is imaged at ~35 km depth below the Neuquén Basin with a local rise to ~30 km at 71°W–69.5°W. The shallowing starts underneath station AS18 and according to the interpretation might be associated with the Loncopué graben. The $v_P/v_S$ ratio with local variation along the profile is shown in Figure 4.5.

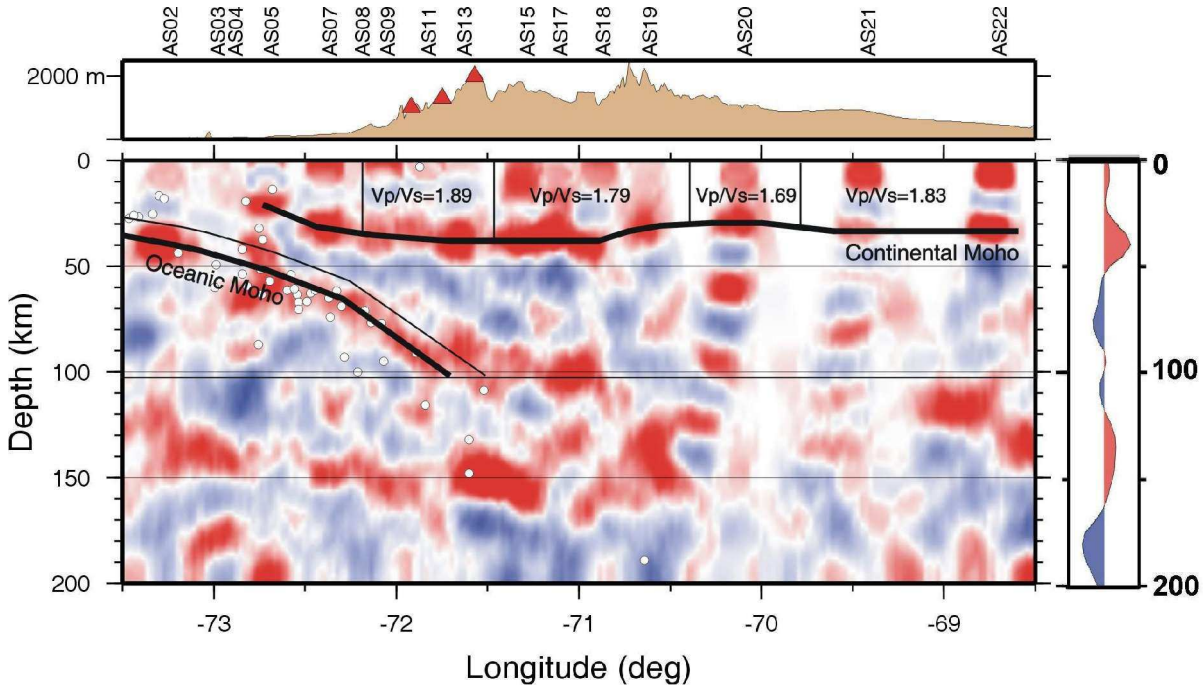


**Figure 4.5**
The receiver function profile at ~39°S (from Yuan et al., 2004, submitted); the upper part shows the broadband stations (AS) and topography (red triangles mark the volcanoes); the lower part of the figure shows the image of the continental Moho and the subducting slab (black lines) with the ISSA hypocentres (white circles). Positive amplitudes are shown in red, and mark shear velocity contrast, with increasing velocity downwards, whereas negative amplitudes (blue) indicate layers with reduced shear wave velocity.

*Summary of the ISSA experiment results*

The ISSA results provide significant information on the structures of the study area at 36°-42°S. These results, summarized below, have been used to constrain the 3D density model.

The upper-crustal seismicity is concentrated in the forearc along the fault zones north and south of the Arauco Peninsula, from a depth of about 5 km to the upper boundary of the lower plate. The Arauco Peninsula itself is almost an aseismic zone, showing also the highest uplift and topography in the forearc region (Bohm et al. 2002). Benioff Zone seismicity is observed down to 150 km depth, with two major maxima at 20 and 60 km. The first of these is attributed to the seismic coupling zone, and the second to the dehydration embrittlement. Relative to the Central Andes, the second maximum is shallower by 40 km (Bohm et al. 2002). From the 2-D velocity model based on the refraction data, the velocities of the arc are higher than those of the forearc.

The presence of the smooth velocity increase below the forearc at depth of approx. 30 km, which is not typical for continental Moho, is either due to the presence of serpentinized mantle or subducted sediments (Bohm et al., 2002; Lüth et al., 2003). However, based on the interpretation of Bohm et al. (2003) and Bohm (2004), low P-wave velocity values that are observed within the uppermost mantle beneath the Coastal Cordillera (at 30-50 km depths) are interpreted as a serpentinized mantle.

The crust/mantle boundary at 40 km depth, as seen from the preliminary receiver-function studies, is in agreement with the global-average continental-arc thickness (Christensen and Mooney, 1995). The west-east velocity variations reflect the structural change from the Palaeozoic accretionary complex that builds the forearc continental crust, to the arc crust intruded by the North Patagonian batholith (NPB). This intrusion took place between the Jurassic and the Neogene. The rocks of the NPB built the Main Cordillera of the southern Andes and are responsible for a higher metamorphic grade than in the forearc region not influenced by the intrusion, leading to observable changes in P-waves velocities in arc and forearc (Bohm et al., 2002).

The Moho is observed at ~39°S latitude at 40 km depth below the main arc, shallowing to 30 km to the east and ~25 km to the west of the arc (Yuan et al., 2004, submitted). However, based on the local earthquake tomography model, the crust/mantle boundary was imaged at 50–55 km depths below the volcanic arc, and ~40 km depths below the Longitudinal Valley (Bohm, 2004).

### 4.2.2 Data from the SPOC experiment

The following summary is based on Krawczyk et al. 2003, unless otherwise stated.

The project Subduction Processes Off Chile (SPOC) was carried out in 2001 as a collaboration between several German and Chilean institutions. The seismic data covering the area of the Chilean subduction system was a combined offshore-onshore, active-passive survey focused on the forearc and the seismogenic-coupling zone. Figure 4.1 shows the offshore profiles of the research vessel Sonne and also the onshore lines. Ten shot-points were located along the near-vertical incidence reflection (NVR) line at ~38°S, the rest at the ends of the W-E profiles. The onshore experiment comprises a pilot NVR and a three dimensional wide-angle reflection/refraction component. The 54 km NVR long profile at 38°15S covers the near-shore part of the subduction zone along the westernmost part of the longer refraction line. The wide angle experiment simultaneously recorded the airgun pulses from the Sonne using 22 OBH/OBS stations along the offshore part of the 38°15S profile, 6 three-component broadband stations along the profile at 39°S and 52 stations along the three W-E profiles at ~36°, 37° and 38°S (one of the velocity profiles is shown in Figure 4.6).

The first results show a non-frontal accretionary system, where thick trench fill seems to have been transported via a subduction channel into the subduction system. The offshore study reveals a strong segmentation of the upper plate and pronounced forearc basins. The velocity profiles show a gradual increase of the P-wave velocity from west to east. Under the Coastal Cordillera and the Longitudinal Valley, the continental Moho was not observed, indicating a smooth transition from continental to oceanic crust (in term of seismic velocities).

These new seismic data also provide the framework for the observed seismicity, which is concentrated in the continental crust and along the ocean-to-continent boundary. Based on both experiments, namely the ISSA and the SPOC, a relocation of the great Valdivia earthquake of 1960 is suggested. This mega-thrust earthquake, according to the SPOC results, was initiated at a latitude of 73°05W, changing the previously suggested position by almost 100 km westwards.

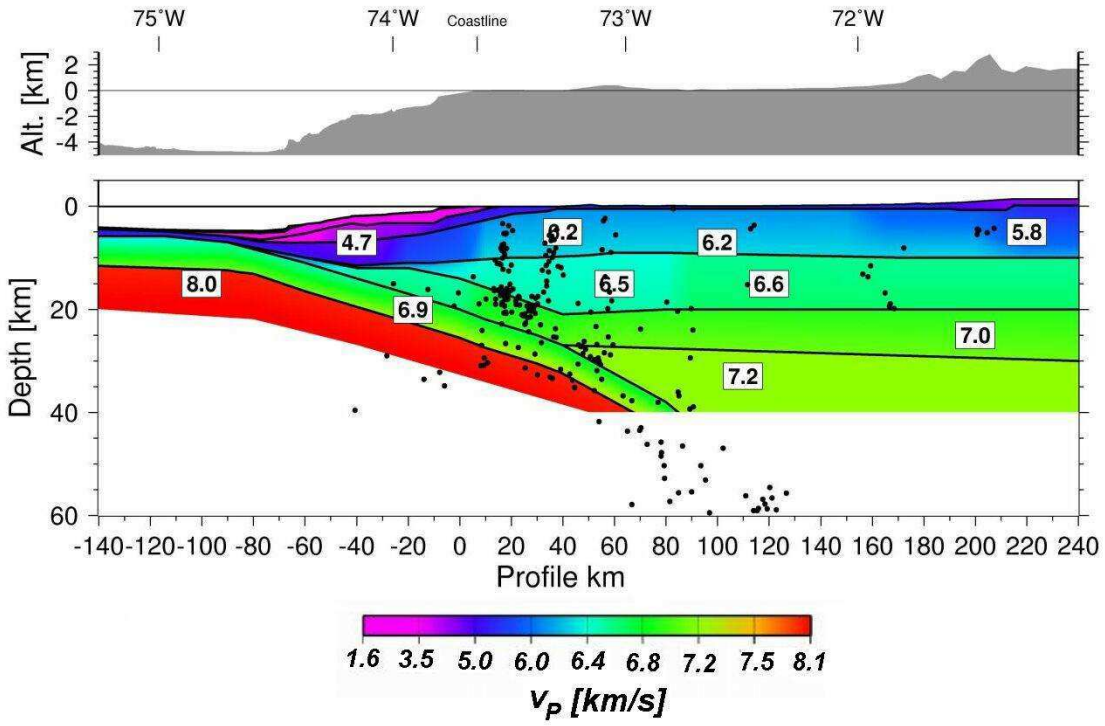


**Figure 4.6**
The SPOC middle 2D refraction line with average velocities of 6.2 km/s in the upper crust and 6.6 – 7.0 km/s in the lower crust. The oceanic crust is characterized by a velocity of 6.9 km/s and the oceanic mantle has a velocity of 8.0 km/s. The black dots denote the earthquakes from the ISSA experiment. The offshore forearc shows slow velocity layers representing the forearc basins (Lüth, S. & SPOC Research Group, 2004).

*Summary of the SPOC experiment results*

Wide-angle reflection/refraction seismic measurements within the framework of the SPOC experiment provide P-wave velocity images along three E-W transects between 36 and 39°S. Near-vertical reflection seismic measurements along the southern SPOC profile at about 38.2°S provide a detailed structural image of the forearc along this profile down to the plate boundary region.

Due to the fact that OBS/OBH instruments recorded the airgun pulses only along the offshore extension of the SPOC south land profile, this is the profile with the best P-wave velocity image of the offshore portion. The westernmost part of the profile crosses the Nazca plate west of the trench and here the crustal thickness of the Nazca plate is 6-7 km. Immediately east of the trench the offshore forearc shows very low P-wave velocities less than 3.5 km/s, possibly due to faulting,

cracking and hydration of this region. The velocities increase to the east so that the upper crustal layer beneath the coastal cordillera has bulk P-wave velocities of 6.0-6.2 km/s along all four profiles. Below this layer P-wave velocities of 6.3-7.0 km/s are found in the lower parts of the continental crust.

Below the SPOC north profile, where the best evidence for the continental Moho has been recognized, the continental Moho rises from about 40 km depth under the western edge of the main cordillera to 25-30 km depth where it meets the plate boundary under the offshore forearc. Associated with this rise in Moho depth is a concomitant decrease in upper mantle P-wave velocity from about 8 km/s to about 7.3 km/s. On the other two profiles, SPOC south and SPOC middle, no evidence for the continental Moho has been observed in the data and the boundary at 30-40 km depth has been marked where velocities of around 7.2 km/s have been reached (Mechie, pers. comm. 2004).

### 4.2.3 Magnetotelluric study

Along two transects near latitude 39°S, long-period magnetotelluric measurements were carried out (Brasse & Soyer, 2001). Long period (T = 10-20000 s) magnetotelluric (MT) stations were deployed at 32 sites between October and December 2000 along E-W profiles from the Pacific coast to the Chilean/Argentinean border. One profile crosses the Coastal Cordillera, Longitudinal Valley and the volcanic arc at a latitude of 38.9°S while the second lies at 39.3°S (Brasse & Soyer, 2001). The 2-D inversion of the MT data revealed three low-resistivity zones below the volcanic arc and Longitudinal Valley. The anomalies B and C in Figure 4.7 below the active Llaima and Villarica volcanoes are situated within the middle to lower crust. A very good conductor (anomaly A, Figure 4.7) on the first profile lies below the Longitudinal Valley at a shallower depth. Both anomalies identified from the northern profile can be associated with the major fault zones (Liquiñe-Ofqui Fault Zone (LOFZ) and the Lahnaluhe (previously referred to as Gastre FZ) Fault Zone), that extend into the lower crust. Anomaly C on the second profile is situated north of the volcanic chain comprising Villarica, Quetrupillán and Lanin volcanoes and may be associated with an upper-mantle high conductivity zone (Brasse & Soyer, 2001; Soyer, 2002).

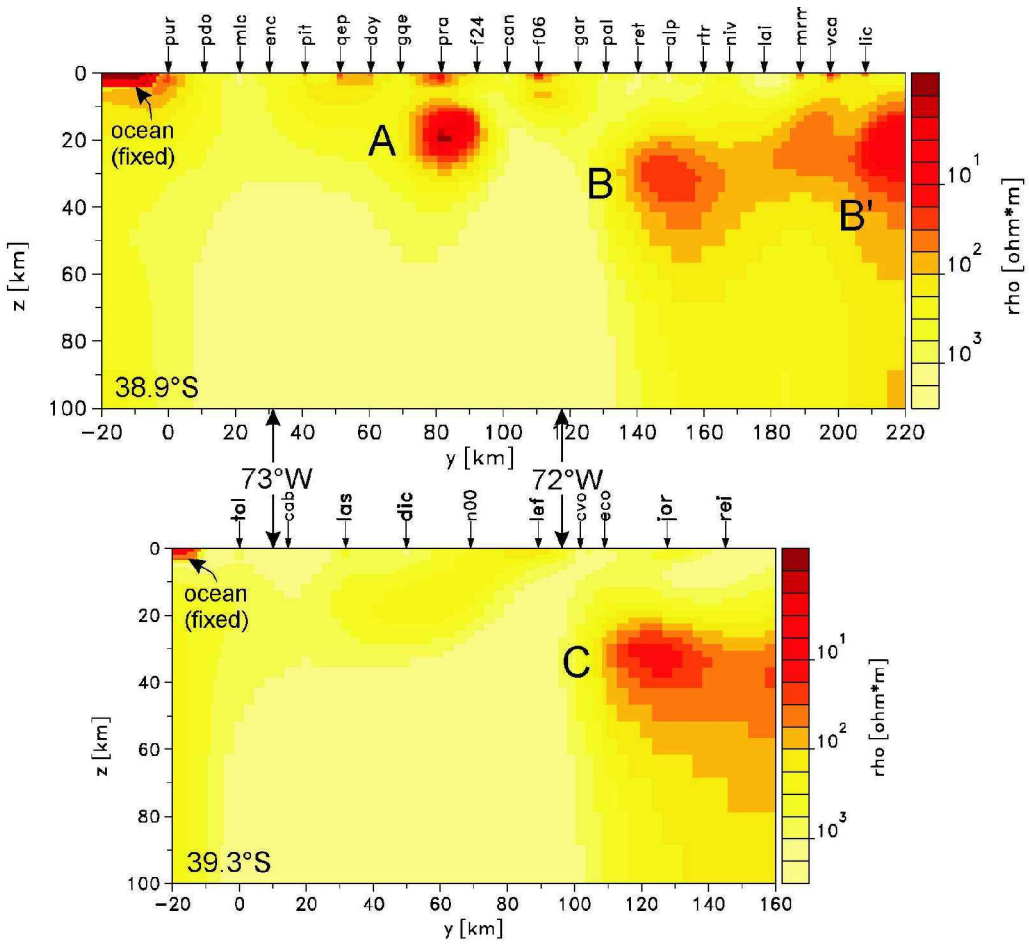


**Figure 4.7**

The three conductors within the crust identified by two magnetotelluric profiles (Brasse & Soyer, 2001); one along the ISSA profile (the upper image) and a southern one at 39.3°S (lower image). Station position and name are indicated by arrows and numbers on the top of both images.

## *4.3 Velocity – Density Relationship*

### 4.3.1 Introduction

Seismic velocities provide fundamental information about rock density, which is obviously the primary input parameter for the density modelling.

The general relationship for the velocity propagation (v) in any material is defined as:

$$v = [\textit{appropriate elastic modulus of material / density of material}]^{1/2}$$

For compressional $v_P$ and shear $v_S$ velocities, density $\rho$ and the elastic moduli (e.g. Kearey & Brooks, 1984):

- **K** - bulk modulus
- $\mu$ – shear modulus

the relationships are given by:

$$v_P = \left[\frac{K + 4/3\mu}{\rho}\right]^{1/2}; \; v_s = \left[\frac{\mu}{\rho}\right]^{1/2} \quad (4.3.1)$$

Laboratory measurements of P-wave velocity and density for more than 3000 igneous and metamorphic rocks under a pressure of 1 GPa (the value representing pressure at a depth of 20 km) suggest the following typical P-wave velocities for different rock types (Christensen & Mooney, 1995):

1. $v_P$ of 6.0 - 6.5 km/s is typical for: granite, diorite, slate, phyllite, amphibolite facies, granitic gneiss, tonalitic gneiss and schist, felsic granulite facies.
2. $v_P$ of 6.5 – 7.0 km/s is typical for: diabase, greenschist facies, basalt, amphibolite and mafic granulite.
3. $v_P$ of 7.0 - 7.5 km/s is typical for: gabbro, mafic garnet granulite.
4. $v_P$ above 7.5 km/s is typical for: pyroxenite, eclogite and dunite.

Based on studies of the physical and chemical properties of various rocks, including laboratory measurements of densities and velocities, relationships between both quantities have been derived. These empirical velocity–density curves, or linear relationships, are called indirect, or in situ methods of density determination. They are usually no more accurate than ±0.01 Mg/m$^3$. They provide a mean density of a particular rock unit, which internally may be quite variable.

### 4.3.2 Indirect methods of density determination

The results of the seismological and seismic experiments SPOC/ISSA, described in previous sections, give information on the geometries of the structures and their velocities. These compressional wave velocities were converted to densities based on the indirect method described in the following section. This method is based on the approach developed by Sobolev & Babeyko (1994).

This approach takes into account in situ temperature and pressure conditions and in three steps converts measured velocities into in situ densities (Sobolev & Babeyko, 1994).

- In the first step, the measured velocities are converted into $v_{P0}$ - velocity under normal conditions ($T_0$=25°C, $P_0$=0.1 MPa):

$$v_{p0} = v_{P(insitu)} - \frac{\partial v_P}{\partial P} P - \frac{\partial v_P}{\partial T}(T - T_0) \quad (4.3.2)$$

where:

$\frac{\partial v_P}{\partial P}$ = 0.12 $\frac{km/s}{GPa}$ (4.3.3) and $\frac{\partial v_P}{\partial T}$ = -4.5 $10^{-4}$ $\frac{km/s}{°C}$ (4.3.4)

- In the second, step the densities $\rho_0$ corresponding to the computed $v_{P0}$ are calculated:

$\rho_0 = 0.446 \times v_{P0} - 0.074$ (4.3.5) for: 6.05 km/s ≤ $v_{P0}$ ≤ 6.95 km/s

$\rho_0 = 0.487 \times v_{P0} - 0.359$ (4.3.6) for: 6.95 km/s ≤ $v_{P0}$ ≤ 7.80 km/s

- The last step converts $\rho_0$ into the in situ densities $\rho$:

$$\rho_{(insitu)} = \rho_0 + \frac{\partial \rho}{\partial P} P + \frac{\partial \rho}{\partial T}(T - T_0) \quad (4.3.7)$$

where:

$\frac{\partial \rho}{\partial P}$ = 0.05 $\frac{Mg}{m^3 GPa}$ (4.3.8) and $\frac{\partial \rho}{\partial T}$ = -9. $10^{-5}$ $\frac{Mg}{m^3 °C}$ (4.3.9)

| | **$V_P$[km/s]** | | |
|---|---|---|---|
| | **SPOC** [km/s] | **ISSA – 39°S** [km/s] | **3-D tomography** [km/s] |
| **Upper crust** | 6.0-6.2 | 5.9 – 6.4 | 5.0-6.5 |
| **Lower crust** | 6.5-7.0 | 6.6-6.9 | 6.5-7.75 |

**Table 4.1**

Representative crustal velocities from the SPOC and ISSA seismic experiments (Bohm, 2004; Lüth et al., 2003).

| Depth[km] | Vp [km/s] | Density (insitu) [Mg/m$^3$] |
|---|---|---|
| **10** | 6.05 | **2.64** |
| **10** | 6.10 | **2.66** |
| **10** | 6.20 | **2.71** |
| **10** | 6.30 | **2.75** |
| **20** | 6.30 | **2.76** |
| **20** | 6.40 | **2.81** |
| **20** | 6.50 | **2.85** |
| **20** | 6.6 | **2.9** |
| **20** | 6.7 | **2.94** |
| **20** | 6.8 | **2.98** |
| **30** | 6.60 | **2.91** |
| **30** | 6.80 | **3.0** |
| **30** | 6.90 | **3.04** |
| **30** | 7 | **3.09** |
| **30** | 7.2 | **3.19** |
| **30** | 7.3 | **3.24** |
| **40** | 7.00 | **3.10** |
| **40** | 7.2 | **3.2** |
| **40** | 7.30 | **3.25** |
| **40** | 7.40 | **3.3** |

**Table 4.2**
Densities for particular depths derived from $v_P$ velocities using equations 3.3.2–3.3.9.

The velocity-density inversion formulas represent a generalized relationship between velocities and densities under certain P/T conditions. These two parameters (P/T) are required input values, which, if not known from a temperature model of the study area, or from heat-flow measurements (from which temperature can be derived), will result in uncertainties in the density estimates. Similarly, the constants used in formula (4.3.5 and 4.3.6) are generalized numbers for the two distinctive rock groups of felsic and mafic composition. They are based on calculations (thermodynamic modelling) of the density and velocity of nine different rock types of various chemical composition (Sobolev & Babeyko, 1994). Therefore, the results of the conversion (Table 4.2) have give the first indications of crustal density values, although other approaches have also been used.

The density of a certain rock is dependent upon its composition and porosity. The petrological – thermodynamic modelling approach, was conducted using “in-house” software (Sobolev & Babeyko, pers. comm., 2004) in order to determine the densities of the lower part of the upper crust and of lower crustal rocks. Thermodynamic modelling is employed to determine the equilibrium mineralogical composition of a rock of a given bulk-chemical composition. The calculated model

proportions and mineral compositions are then used to calculate density (see Figure 4.8) and the isotropic elastic wave velocities of the rock (Sobolev & Babeyko, 1994). The chemical composition used for the density determination within the study area is based on published data and was carried out for this study region as well as for a different density model developed for an area north between latitudes 26°S-37°S (Tassara, pers. comm.).

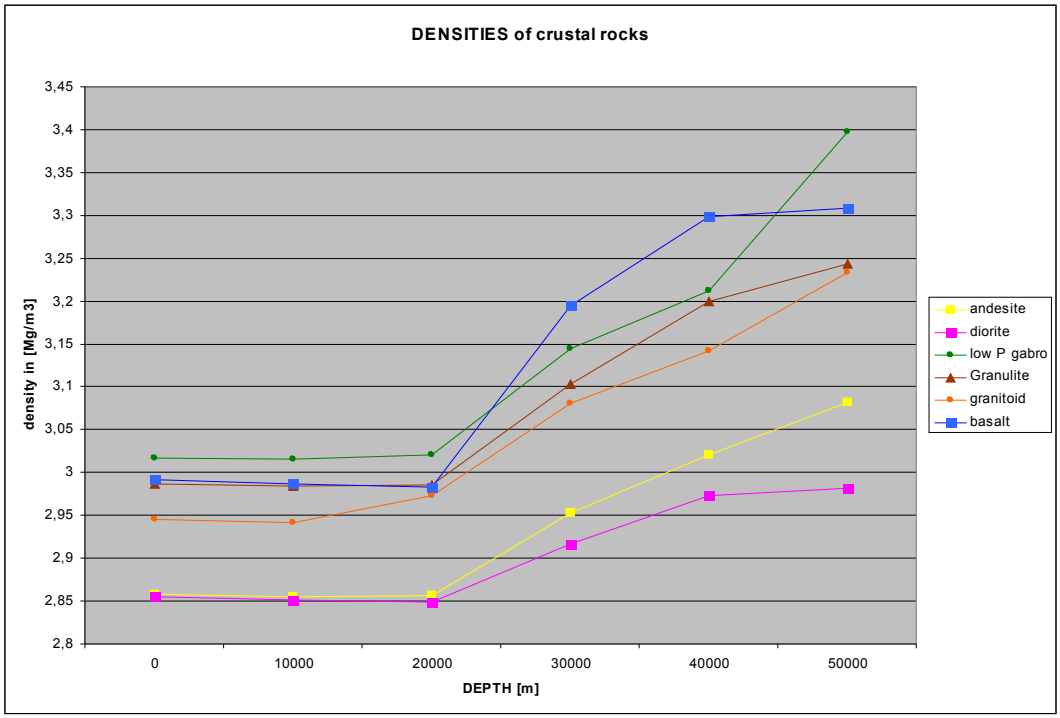


**Figure 4.8**
The density values of six different crustal rocks for the depth range 0–50 km computed using the Sobolev-Babeyko program.

Additional results are listed in Table 4.3, where they are compared with the results of the second approach used, namely that of Hacker et al. (2003). This method uses the results of a new compilation of the physical properties of the minerals making up the most abundant rock compositions relevant to subduction zones, such as mid-ocean ridge basalt (MORB), lherzolite, depleted lherzolite, harzburgite and serpentinite (Hacker et al., 2003). Various rock types can be examined, however their mineralogy must be known. For each rock composition, the P-T stability fields of different minerals are calculated. The data is then used to compute the water content, density and seismic wave speed of the subduction zone rocks as a function of P and T (Hacker et al., 2003).

| | HACKER ET AL. | | | SOBOLEV & BABEYKO | | |
|---|---|---|---|---|---|---|
| DEPTH [km] | $^{V}P$ [km/s] | ρ [Mg/m$^3$] | ROCK | ROCK | $^{V}P$ [km/s] | ρ [Mg/m$^3$] |
| | 6,03 | 2,7 | Granitic gneiss | | | |
| 10 | 6,19 | 2,67 | Granit | | | |
| | 6,33 | 2,67 | Granit s&b | | | |
| | 6,33 | 2,77 | Granodiorite | | | |
| | 6,47 | 2,81 | Tonalite | | | |
| | 6,19 | 2,68 | Granit | | | |
| | 6,33 | 2,78 | Granodiorite | | | |
| 20 | 6,5 | 2,81 | Tonalite | RF-MdC | 6,39 | 2,81 |
| | 6,57 | 2,83 | Diorite | SB-Diorite | 6,49 | 2,85 |
| | 6,59 | 3,02 | Amphibolite facies | P88 granitoid | 6,87 | 2,97 |
| | 6,51-6,57 | 2,83 | Tonalite-diorite | (SB-Diorite) | 6,57 | 2,92 |
| | 6,6 | 3,03 | Amphibolite facies | | | |
| | 6,67-6,84 | 3,04 | Gabbro | gabbroHV | 7,16 | 3,07 |
| | 6,79 | 3,11 | Granulite facies | mafic cumul. | 7,01 | 3,07 |
| 30 | 6,8 | 2,89 | Felsic granulite | UZ1Em.granulite | 7,07 | 3,2 |
| | 6,98 | 2,99 | Cpx-granulite | granuliteJK | 7,09 | 3,1 |
| | 7 | 2,9 | LherzoliteQ(29%serp.) | | | |
| | 7,2 | 3,05 | Olivin-granulite | granuliteHV95 | 7,15 | 3,25 |
| 35 | 7,81 | 3,3 | Lherzolite D | RF-Gr.Int.T | 6,55 | 2,93 |
| | 6,7-6,8 | 3,05 | Gabbro | | | |
| | 6,98 | 2,99 | Cpx-granulite | UZ1Em.granulite | 7,11 | 3,23 |
| | 7,21 | 3,05 | Olivin-granulite | mafic cumul. | 7,23 | 3,19 |
| 40 | 7,4 | 3,3 | Garnet-granulite | RF-Gr.Mf.T | 7,24 | 3,22 |
| | 7,79 | 3,3 | Lherzolite D | | | |
| | 8,12 | 3,3 | Harzburgite | RF-LCCtr | 6,56 | 2,99 |
| | 8,22 | 3,24 | Lherzolite A | | | |
| | 6,99 | 2,92 | LherzoliteQ(29%serp.) | | | |
| | 7,77 | 3,29 | Lherzolite D | | | |
| 50 | 8,13 | 3,3 | Harzburgite | | | |
| | 8,22 | 3,24 | Lherzolite A | | | |
| | 8,23 | 3,31 | Dunite | | | |

**Table 4.3**

Using the velocity values from the SPOC and ISSA results, specific rock types of given mineralogical and chemical composition, were identified according to the calculated velocity values at same depths. The calculation was performed using the two described methods (Hacker et al., 2004; Sobolev & Babeyko, 1994). The attempt was to link observed velocity values to possible composition at a certain depth.

## References for the rocks in Table 4.3:

**RF-MdC**- mid-crust contractional orogens, Rudnick & Fountain, 1995
**SB**-diorite, Sobolev&Babeyko, 1994
**P88 –773R** granitoid, Parada et al., 1988
**HV95-193** – gabbro, Hickey-Varas et al., 1995
**VK-V45** –mafic/ultramafic cumulates (arc-backarc); Vujovich & Kay, 1998
**UZ1E**- mafic granulite, Kay, 1996
**JK01-Gr**- granulite, Jull & Kelemen, 2001
**HV95-3238-2f** – granulite, Hickey-Varas et al., 1995
**RF-GrIntTr**- granulitic intermediate terrain, Rudnick& Fountain, 1995
**RF-GrMfTr**- granulitic mafic terrain, Rudnick& Fountain, 1995
**RF-LCCtr-** low crust contractional orogens, Rudnick & Fountain, 1995

### 4.3.3 Problems associated with indirect density determination

*1. Disadvantages of the approaches used*

The density and/or velocity of given rocks with their chemical or mineralogical composition are then calculated along a geotherm. The approach of Hacker et al. (2004) does not take into account mineral reactions occurring at each depth with changing pressure and temperature. These reactions change mineral assemblages from plagioclase-bearing and garnet-free to garnet-bearing and plagioclase-free. Both have a strong influence on densities, and obviously not taking them into account is a limitation of this approach. For example, results from the thermodynamic modelling of Sobolev and Babeyko (1994) (Figure 4.8) show at 20 km depth a tremendous increase in the densities of all considered rocks, whereas the trend in the density values computed by the Hacker et al. (2004) method (Figure A.1) remains rather linear and only depth and P/T dependent. On the other hand, the Sobolev and Babeyko approach was done for several anhydrous magmatic rocks of a broad compositional variety (from granite to lherzolite). However, not considering water content may be a limitation of this method.

*2. Determination of temperature and pressure*

The P/T values are required input parameters for the methods described and applied. The biggest problem in determining densities, especially for the mantle (oceanic and continental) and the oceanic crust, is the degree of freedom available when choosing the various required parameters (temperature, pressure and composition). Apart from information dealing with the plate age, there are no other geophysical or petrological constraints on the temperature and composition of the subducting slab in this specific region. In both methods used for density calculation, formulas B.1-B.5 were used for P/T determination. Having a thermal model computed for the study area would provide certain constraints on the possible composition of the subducted oceanic crust and mantle. The thermal model of Oleskevich et al. (1999) (Figure B.1), compared with the thermal and petrological models estimated for the Japanese subduction zone (Figure B.2), provides some

initial estimates for the possible densities and compositions related to different depths, P/T conditions and mineralogical reactions occurring within the slab as it subducts.

*3. Required compositional information*

The densities of crustal rocks are dependent upon the chemical or mineralogical composition of the given rocks. If composition is not known from samples available in the study area, published data must be used. These data are limited, and therefore the best representatives for the whole regions are difficult to identify.

Also, in the database of the Hacker et al. (2003) method used to estimate the densities, there are more than 27 different ultramafic mantle rocks (harzburgites and lherzolites, with different mineralogical composition) giving a range of possible density values between 2.7 and 3.41 $Mg/m^3$.

Results from the density computations were used at the beginning of the density modelling to allocate approximate density values of the geological structures within the 3D model. Later, they were modified (the upper-crustal densities were partly constrained by the density measurements (Section 4.3.4) and geological information (Chapter 2)); but the range of possible densities in relation to depth and P/T conditions (especially for the mantle rocks) has remained consistent with the previous results.

The resulting density values within the density model will be discussed in greater detail in Chapter 5.

### 4.3.4 Direct methods

Apart from the indirect methods, direct density measurement were also carried out. The densities of 21 samples of different rocks were derived from measuring their weight in air ($m_{Air}$) and in water ($m_{Water}$). The differences between the weights in air and water were divided by the density of the water (0.998 Mg/m$^3$), giving in the volume of water displaced by the sample the resulting sample density given by :

$$\rho = \frac{mass}{volume} = \frac{m_{Air}}{(m_{Air} - m_{Water}) / \rho_{Water}} \Rightarrow \rho_{measured} = \frac{0.998 * m_{Air}}{(m_{Air} - m_{Water})} \text{ [Mg/m}^3\text{]} \quad (4.3.15)$$

Sample densities determined in this way are shown in Table 4.4.

| MEASURED DENSITIES (18.3. 2004) | | | | | | | |
|---|---|---|---|---|---|---|---|
| 1 | 2 | **Weight** | **Weight(1)** | **Weight(2)** | 1+2 | **density** | **location** |
| **sample** | **name** | **In air [g]** | **in water [g]** | **in water [g]** | **[g]** | **[Mg/m$^3$]** | Latitude, Longitude |
| ANG1 | Nahuelbuta granite | 934,78 | 300,33 | 291,85 | 592,18 | **2,723** | 37°52'S, 72°45'W |
| FLO1 | Nahuelbuta granite | 202,82 | 63,17 | 64,58 | 127,75 | **2,696** | 36°46'S, 72°48'W |
| LAR1 | Eastern series metasediment | 524,53 | 163,22 | 167,25 | 330,47 | **2,698** | 37°12'S, 73°10'W |
| LAR2 | Eastern series metasediment | 243,73 | 77,24 | 75,69 | 152,93 | **2,679** | 37°12'S, 73°10'W |
| PCB | Western series metabasite | 664,75 | 228,61 | 217,86 | 446,47 | **3,039** | 39°43'S, 73°24'W |
| VAL 6d | Western series metabasite | 236,37 | 77,53 | 80,21 | 157,74 | **3,000** | 39°43'S, 73°24'W |
| VAL 31 | Western series metabasite | 344,61 | 111,98 | 109,94 | 221,92 | **2,803** | 38°15'S, 73°30'W |
| PCB 1 | Western series metabasite | 231,16 | 76,07 | 78,63 | 154,7 | **3,017** | 39°43'S, 73°24'W |
| **LAH1?** | Western series metasediment | 471,25 | 148,25 | 150,21 | 298,46 | **2,722** | 38°03'S, 73°22'W |
| VAL 37 | Western series metasediment | 356,49 | 111,08 | 109,52 | 220,6 | **2,618** | 40°32'S, 73°43'W |
| VAL 42 | Western series metasediment | 546,44 | 175,85 | 171,72 | 347,57 | **2,742** | 40°35' S, 73°44' W |
| VAL 27 | Western series metasediment | 353,54 | 113,09 | 111,04 | 224,13 | **2,726** | 38°13' S, 73°28' W |
| VAL 49 | Western series metasediment | 995,57 | 312,9 | 307,96 | 620,86 | **2,652** | 41°48°S, 74°01'W |
| LOF 147 | Magmatic arc diorite-gabbro | 652,7 | 219,02 | 206,45 | 425,47 | **2,867** | 38°02'S, 71°44'W |
| LOF 149 | Magmatic arc- granodiorite | 888,18 | 286,35 | 279,9 | 566,25 | **2,753** | 38°36'S, 71°26'W |
| LOF 164 | Magmatic arc-diorite mikrogr. | 812,9 | 256,6 | 248,59 | 505,19 | **2,636** | 38°36'S, 71°00'W |
| LONG 1 | Magmatic arc- syenit | 228,42 | 68,81 | 70,73 | 139,54 | **2,565** | 38°50'S, 71°25'W |
| LONG 2 | Magmatic arc- granite | 237,9 | 71,73 | 73,69 | 145,42 | **2,567** | 38°51'S, 71°30'W |
| LOF 135 | Magmatic arc- granite | 726,99 | 223,36 | 224,18 | 447,54 | **2,596** | 39°03'S, 71°48'W |
| LOF 17 | Magmatic arc- granite | 981,73 | 304,93 | 298,42 | 603,35 | **2,589** | 39°47'S, 71°50'W |
| LOF 10 | Magmatic arc- granite | 835,44 | 263,88 | 259,5 | 523,38 | **2,672** | 39°42'S, 71°54'W |

**Table 4.4**
Measured rock densities for samples from the forearc (13) and volcanic arc (8).